IEEE Access
Multidisciplinary | Rapid Review | Open Access Journal

Received December 4, 2018, accepted December 8, 2018, date of publication December 12, 2018,
date of current version January 7, 2019.

Digital Object Identifier 10.1109/ACCESS.2018.2886252

Analysis of Morphing Modes of Hypersonic Morphing Aircraft and Multiobjective Trajectory Optimization

WUYU PENG, TAO YANG, ZHIWEI FENG, AND QINGBIN ZHANG
College of Aerospace Science and Engineering, National University of Defense Technology, Changsha 410073, China
Corresponding author: Tao Yang (taoy90@163.com)

ABSTRACT Aiming at improving the range of wing-body combination aircraft at hypersonic flow conditions and exploring the application of morphing technology in hypersonic aircraft, morphing aircrafts with different morphing modes have been proposed. The aerodynamic characteristics and wing efficiency of morphing aircraft with different morphing modes have been studied for a further application. In order to verify the significance of morphing technology on the trajectory, the trajectory of the glide phase has been optimized through multiobjective optimization method. Through a 3 degree-of-freedom dynamic model and a heat flux model, the range of glide trajectory and the total heat of the leading edge of the wing are calculated and selected as optimization objectives in the multiobjective optimization problem. The optimization variables include the Mach numbers when the aircraft is morphing (morphing timing) and the angle of attack of different phases. Based on the multiobjective evolutionary algorithm based on decomposition, the multiobjective trajectory optimization problem is solved and a uniform Pareto Front is obtained, and through the analysis of typical solutions, it can be seen that a compromise is made to balance the two objectives. Through the comparison of morphing and non-morphing aircraft, morphing aircraft can fly further with a smaller total heat of the leading edge of the wing. Also, it seems that the variable sweep wing morphing mode has a better overall performance. The result in this paper is a verification of the application prospects of the morphing technology under hypersonic environment, which will provide a reference for further application of morphing technology in hypersonic aircraft.

INDEX TERMS Morphing aircraft, hypersonic, aerodynamic performance, trajectory optimization, MOEA/D.

I. INTRODUCTION

The increasingly complex mission requirements and flight environment have imposed increasingly higher requirements on the performance of the aircraft, forcing the flight envelope to gradually expand, and the concept of morphing aircraft has emerged. The morphing aircraft is a multi-purpose and multi-modal aircraft that can be adaptively deformed according to the flight environment, flight profile, and mission requirements. The trajectory, flight altitude, and flight speed of the morphing aircraft are maneuverable, and the flight conditions are diverse (such as take-off and landing, cruising, maneuvering, hovering, and diving, etc.). The aircraft can be used to perform various missions under different flight conditions to optimal flight performance [1]–[4].

Compared with traditional aircraft, morphing aircraft can improve the flight performance through morphing, broaden the stable working range with different height and velocity, it has advantages such as strong maneuvering ability, wide range of working space and good control quality [5]–[7]. Due to its outstanding overall performance, with the development of related disciplines such as smart materials and structures, the research on morphing aircraft is in full swing all around the world, however most of them are aimed at developing morphing aircraft under low speed conditions [8]. There are relatively few researches on morphing aircraft applied to transonic to supersonic speeds. Among the ''Morphing Aircraft Structures'' (MAS) project conducted by the Defense Advanced Research Projects Agency (DARPA) in the United States, three contractors have carried out different morphing design. With the further funding from DARPA, the corresponding prototype development and wind tunnel tests were carried out. The three contractors contracted the

contractual requirements of the project by using morphing modes of telescoping, skin sweeping and three-dimensional folding [9]–[11]. Bae [12], [13] analyzed the cruise aerodynamic characteristics and structural characteristics of a variable-span morphing wing aircraft. Chen [14] made a comparative analysis of two variable-sweep modes of morphing wing in subsonic condition. Gao [15] and Huanhuan [16] analyzed the aerodynamic characteristics of the Z-folding wing and the variable-span variable-sweep wing morphing aircraft at subsonic and transonic conditions, then carried out the corresponding trajectory optimization design and simulation. Guo *et al.* [17] studied the aerodynamic characteristics and dynamic characteristics of asymmetric telescopic wing aircraft. Leahy [18], Burdette *et al.* [19], and Afonso *et al.* [20] did some optimization on profile and morphing mode on morphing aircraft to improve performance. He *et al.* [21] proposed a TP model-based modeling and control design approach for morphing aircraft undergoing shape change. Michaud [22], Gabor [23], and Koreanschi *et al.* [24], [25] optimized and designed a morphing wing-tip demonstrator for drag reduction at low speed, through the wind tunnel test it shows good aerodynamic and structural properties. Ermakova and Dayyani [26] optimized the shape of composite corrugated morphing skins for low speed. Although there are many researches on morphing aircraft, most of them are focused on subsonic and transonic conditions, and there is little to learn about morphing aircraft in supersonic and hypersonic environments. Also, the review of the mechanics of composite corrugated structures by Dayyani *et al.* [27] and the survey of skin design for morphing wing aircraft by La *et al.* [28] shows the possibility of applying morphing wing to hypersonic aircraft.

Considering that the hypersonic flow is different from the subsonic and transonic flow, this paper analyzed the morphing aircraft under supersonic and hypersonic conditions. Due to the influence of the harsh force and thermal environment on the reliability of the morphing mechanism under hypersonic condition, the morphing is only developed in the two-dimensional plane. For the three morphing modes of telescopic wing, variable sweep wing and two-dimensional folding wing, the aerodynamic characteristics are compared. The surface efficiency and stability characteristics are analyzed to compare the advantages and disadvantages of different morphing modes under hypersonic conditions. To explore the application of morphing technology in hypersonic aircraft, a typical morphing mode is selected to study the glide trajectory of hypersonic morphing aircraft. Because of the conflict between the targets, this paper adopts the multiobjective optimization method to optimize the flight trajectory. At present, most of the multiobjective evolutionary algorithm (including NSGA-II [29] which is more commonly used in the design of aircraft) use populations for multi-point search, and the adaptive specified strategy based on Pareto dominance is used to obtain the approximate PF. Although it is successfully used in engineering design, there are still difficulties in maintaining diversity. In 2007, Zhang and Li presented MOEA/D [30], with the advantages of simple evolution mechanism, fast convergence speed and relatively uniform edge of Pareto, it has been widely used in recent years [31]–[33].

In our previous work, we have discussed the trajectory optimization problem of varied sweep wing morphing aircraft briefly [34], the variable sweep wing morphing mode was applied in hypersonic aircraft, aerodynamic performance, mainly lift-to-drag ratio (the amount of lift generated by the aircraft, divided by the aerodynamic drag it creates by moving through the air, denotes by L/D) was briefly introduced, and then a multi-objective trajectory optimization problem was proposed to optimize the range and the total heat at the leading edge of the wing. The work shows that the variable sweep wing morphing mode can be used in hypersonic aircraft to improve the over all performance. However, there are many kinds of morphing modes have been used in subsonic and transonic conditions, in this paper, different morphing modes are applied to hypersonic aircraft, and the effect of different modes are compared in different aspects. The result in this paper is a verification of the application prospects of morphing technology under hypersonic environment. It also shows that, among all the three morphing modes discussed in the paper, variable sweep wing morphing mode has a better overall performance.

The structure of the paper is arranged as follows. In Section.II, different kinds of morphing mode of wing are introduced firstly, in Section.III, a 3-DoF dynamic model and a leading edge heat model of glide trajectory are established. Then a multiobjective optimization model of the morphing aircraft trajectory is carried out in Section.IV. In Section.V, the lift-to-drag ratio, wing efficiency and stability are given and compared under different morphing conditions. Finally in Section.VI, MOEA/D is used to optimize the glide trajectory. The optimized PF is analyzed, and both the range and the total heat absorption of leading edge are compared.

II. MORPHING MODES

Under high-speed conditions, morphing of the aircraft through the wing can improve the overall performance from the aspects of survivability, maneuverability, and expand the flight envelope of the aircraft. The reference profile studied in this paper is a typical face-symmetrical wing assembly shape, as shown in Fig.1. The main body of the aircraft is a conical column assembly, trapezoidal lift wings are on both sides, and the ''+'' air rudders are located at the tail of the aircraft.

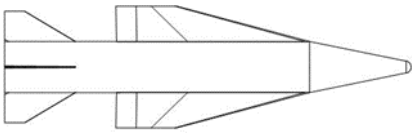

FIGURE 1. The reference profile.

Due to the large-scale morphing of the wing, the aerodynamic characteristics and flight control of the aircraft are greatly affected. Considering the difficulty of engineering

implementation, most of the currently used morphing wings adopt rigid morphing mode [5]. In order to improve the flight performance of the aircraft, the trapezoidal wing is considered to be deformed in the two-dimensional plane, considering the harsh force and thermal environment under hypersonic environment. Three morphing modes are mainly considered: telescopic wing, variable sweep wing and folding wing. The morphing process and the profile after morphing are as follows.

The telescopic morphing wing mode is achieved by a sleeve structure mounted in a trapezoidal lift wing. One or more stages of extension can be performed as the mission changes, similar to the prototype of Raytheon's MAS project for DARPA [5], as shown in Fig.2. The telescopic wing morphing profile based on the reference shape is shown in Fig.3.

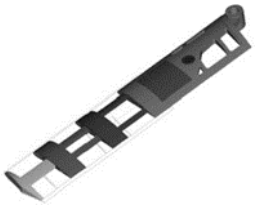

FIGURE 2. Raytheon's telescopic wing morphing project.

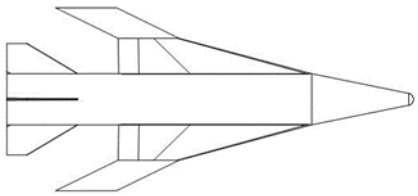

FIGURE 3. The telescopic wing morphing profile.

The variable sweep wing morphing process uses a shear morphing method to change the leading edge angle of the trapezoidal wing, that is, to change the wingtip chord length to adapt to different angles by changing the leading edge's sweep angle on the basis of maintaining the aircraft's wingspan. During the flight, the wing of the aircraft only changes in chord direction, as shown in Fig.4 below.

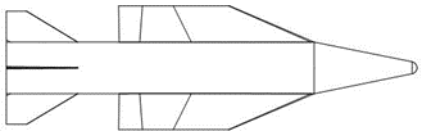

FIGURE 4. The variable sweep wing morphing profile.

The folding wing morphing mode is done in the two-dimensional plane. By folding, the original trapezoidal wing rotates around the leading wing root point, and the folding wing is expanded to increase the lift-to-drag ratio. The folding wing morphing mode mainly achieves the purpose of increasing the lift force by changing the sweep angle and increasing the span. The morphing process is shown in Fig.5. By further amendment, the folding wing morphing profile is shown in Fig.6.

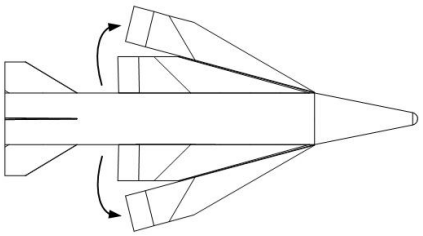

FIGURE 5. The process of folding morphing.

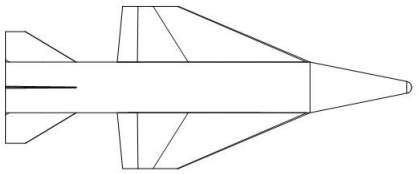

FIGURE 6. The folding wing morphing profile.

III. TRAJECTORY / HEAT FLUX MODEL

Assuming that the earth is a rotating sphere and the sideslip angle is zero, 3-DoF motion model of the unpowered glide trajectory of the morphing aircraft is as Equation (1) [35]:

$$\begin{cases} \dot{V} = -\dfrac{D}{m} - g_m \sin\vartheta \\ \quad +\omega_m^2 r\cos\phi(\sin\theta\cos\phi - \cos\vartheta\cos\sigma\sin\phi) \\ \dot{\theta} = \dfrac{L\cos\nu}{mV} + \left(\dfrac{V}{r} - \dfrac{g_m}{V}\right)\cos\vartheta + 2\omega_m\cos\phi\sin\sigma \\ \quad +\dfrac{\omega_m^2 r\cos\phi}{V}(\cos\vartheta\cos\phi + \sin\vartheta\cos\sigma\sin\phi) \\ \dot{\sigma} = \dfrac{L\sin\nu}{mV\cos\vartheta} + \dfrac{V\cos\vartheta\sin\sigma\tan\phi}{r} \\ \quad +\omega_m^2 r\dfrac{\sin\sigma\sin\phi\cos\phi}{V\cos\vartheta} \\ \quad -2\omega_m(\cos\phi\tan\vartheta\cos\sigma - \sin\phi) \\ \dot{\phi} = \dfrac{V\cos\vartheta\cos\sigma}{r} \\ \dot{\lambda} = \dfrac{V\cos\vartheta\sin\sigma}{r\cos\phi} \\ \dot{r} = V\sin\theta \end{cases} \tag{1}$$

The position parameters are described by the three parameters of earth center distance r, longitude λ and latitude ϕ, and the speed parameters are the speed V, velocity inclination angle ϑ (the angle between the velocity vector and the local horizontal plane, the velocity vector is positive when pointing above the horizontal plane) and the velocity deviation angle σ (the angle between projection of the speed vector on local horizontal plane and the true north direction, which is positive when it is clockwise from north direction to the speed vector). D and L respectively represent drag and lift, g_m is gravity acceleration, $\omega_m = 7.292\times10^{-5}$ rad/s is the angular velocity of the earth's rotation, ν is the angle of inclination, indicating

the angle between the lift direction and the vertical plane containing the velocity vector, looking from the rear of the aircraft forward, if the direction of lift is tilted to the right, then the angle is positive.

Unlike ordinary aircraft, which mainly estimates the heat flow at the stagnation point. Because the morphing aircraft adopts a variable sweep wing morphing mode, the leading edge of the morphing wing is one of the most heated components during the pulling up and glide process. Therefore, in addition to the head stagnation point, more consideration should be given to the effect of heat protection on the reliability of the morphing mechanism. During the flight process, the total heat absorption at the leading edge of the wing is determined by estimating the heat flux at the leading edge of the wing.

Regardless of the interference effect of the aircraft body on the morphing wing, the aerodynamic heating of the leading edge of the wing can be calculated approximately according to the heat flux formula for the leading edge of the sweepback cylindrical wing [36], as Equation (2).

$$q_x = \alpha \left(T_{w\Lambda} - T_w\right) \tag{2}$$

Parameters in Equation (2) can be calculated through Equation (3)-(7), Λ is the sweep angle of the morphing wing.

$$T_{w\Lambda} = \mathrm{Pr}^{0.5}\left(T_{\infty 0} - T_{N0}\right) + T_{N0} \tag{3}$$

$$T_{\infty 0} = T_\infty \left(1 + \frac{\gamma - 1}{2} Ma_\infty^2\right) \tag{4}$$

$$T_{N0} = T_\infty \left(1 + \frac{\gamma - 1}{2} Ma_\infty^2 \cos^2 \Lambda\right) \tag{5}$$

$$\theta_w' = \left[1 + 1.5\left(\theta_{w0}'\right)^{3.5} T_w / T_{\infty 0}\right] \theta_{w0}' \tag{6}$$

$$\alpha = \theta_{\mathrm{w}}' \mathrm{Pr}^{-0.54} \left(\rho\mu\right)_{w\Lambda}^{0.5} \left(\frac{du}{dx}\right)_{SL}^{1/2} C_p \tag{7}$$

The density $\rho_{w\Lambda}$ is obtained from the thermodynamic function table based on the total pressure $p_{WSL\Lambda}$ at the leading edge of the wing and the recovery temperature $T_{w\Lambda}$.

Velocity gradient du/dx is represented by a piecewise function.

$$\frac{du}{dx} = \begin{cases} \dfrac{A_0 - B_0}{0.7} Ma_{N\infty} & \\ -\dfrac{0.8A_0 - 1.5B_0}{0.7} & (0.8 < Ma_{N\infty} < 1.5) \\ \dfrac{1}{R_0}\left[\dfrac{2\left(p_{WSL\Lambda} - p_\infty\right)}{\rho}\right]^{0.5} & (Ma_{N\infty} \geq 1.5) \end{cases} \tag{8}$$

In Equation (8), the parameters can be calculated through the equations below,

$$Ma_{N\infty} = Ma_\infty \cos \Lambda \tag{9}$$

$$A_0 = \frac{1}{R_0}\left[\frac{2\left(p_{WSL\Lambda} - p_\infty\right)}{\rho}\right]_{Ma_{N\infty}=1.5}^{0.5} \tag{10}$$

$$B_0 = \left[\frac{2u_{\infty\Lambda}}{R_0}\left(1 - 0.416Ma_{N\infty}^2 - 0.164Ma_{N\infty}^4\right)\right]_{Ma_{N\infty}=0.8} \tag{11}$$

$$p_{WSL\Lambda} = \begin{cases} p_\infty \left(1 + \dfrac{\gamma - 1}{2} Ma_{N\infty}^2\right)^{\gamma/\gamma - 1} & (Ma_{N\infty} < 1) \\ p_\infty \left(\dfrac{\gamma + 1}{2} Ma_{N\infty}^2\right)^{\gamma/\gamma - 1} / & \\ \left[\dfrac{1 + \gamma}{2\gamma Ma_{N\infty}^2 - (\gamma - 1)}\right]^{1/\gamma - 1} & (Ma_{N\infty} \geq 1) \end{cases} \tag{12}$$

Combining Sutherland equation and gas state equation with the above equations, the heat flux at the leading edge of the wing can be calculated, and the total heat Q absorption of the leading edge of the morphing wing during flight can be obtained through integration.

IV. MULTIOBJECTIVE OPTIMIZATION MODEL OF THE MORPHING AIRCRAFT TRAJECTORY

When establish a multiobjective optimization model for a morphing aircraft trajectory, it is necessary to comprehensively consider the design requirements of the morphing aircraft, select an appropriate objective function to meet the mission requirements and the thermal restrictions during the flight, take into account the morphing process and the state variables during the flight to determine the design variables.

A. OBJECTIVE FUNCTION

The primary task of optimization of the glide trajectory of the morphing aircraft is to make the glide trajectory as long as possible under the restrictions. This requires that after pulling up, the morphing aircraft should be in the state of maximum lift-to-drag ratio (L/D) as long as possible, and the morphing mechanism should be reliable in the severe thermal environment of hypersonic and supersonic environment.

Considering the above requirements, this paper selected the range of the glide trajectory R and the total heat absorption at the leading edge of the morphing wing Q as the objective function. The larger the range of the glide trajectory, the better the effect of morphing on increasing the range of the aircraft; the smaller the total heat absorbed by the leading edge of the morphing wing, the more beneficial it is to protect the internal morphing mechanism of the wing from being damaged.

In summary, the multiobjective optimization model for the trajectory optimization of a morphing aircraft is as Equation (13).

$$F = \left(\max f_1 = R, \min f_2 = Q\right) \tag{13}$$

B. DESIGN VARIABLES

For the ordinary trajectory optimization problem, the optimization of trajectory is mainly accomplished through the adjustment of the ballistic parameters. Generally, the parameters that have a greater impact on the optimization target in the ballistic parameters are selected as design variables, such as the angle of attack and the velocity inclination. However, for trajectory optimization of a morphing aircraft, in addition to the ballistic parameters, the choice of morphing timing also has a great influence on the objective functions, especially

the range. Therefore, in the trajectory optimization problem of a morphing aircraft, the design variables are mainly determined from the two aspects of morphing timing and ballistic parameters.

In different phases of the trajectory, the trajectory equations depend on the morphing profile through the lift and drag, and the heat equations depend on the morphing profile through the angle of attack and the sweep angle of the morphing wing. So the morphing timing is chosen as design variable.

As the morphing aircraft adopts a two-stage variable sweep wing morphing mode. Therefore, the morphing Mach numbers are selected as the design variables for determining the timing of morphing. The Mach number when the aircraft deforms to the first stage variable sweep wing profile is $\boldsymbol{M}_1$, in the similar way $\boldsymbol{M}_2$ is defined.

In the trajectory optimization problem studied in this paper, the aircraft only moves in the longitudinal plane, the maximum range can be achieved if the maximum lift-to-drag ratio is maintained at all times. However, for the heat flux of the wing leading edge, it can be seen in Equation (2) that the heat flux and AoA are positively correlated.

The maximum value of lift-to-drag that can be obtained by changing AoA, so does the total heat absorption at the leading edge of the morphing wing. Therefore, the trajectory optimization model mainly considers AoA during flight as design variable, represented by α.

Because the morphing aircraft has a two-stage variable sweep wing morphing mode, the aircraft fly in three different morphing modes during the unpowered glide trajectory. In order to simplify the calculation, it is assumed that AoA in each modes changes linearly, the unique angle of attack curve can be determined by the starting and ending values of each angle of attack command. The starting and ending AoA in three modes are represented by α_1 to α_6 in sequence.

In summary, the design variables of the morphing aircraft trajectory optimization model can be expressed as Equation (14).

$$x = (M_1, M_2, \alpha_1, \alpha_2, \alpha_3, \alpha_4, \alpha_5, \alpha_6)^T \tag{14}$$

C. RESTRICTIONS

In the optimization problem discussed here, the restrictions mainly consist of the scope of morphing time, the range of values of the ballistic parameters and the ballistic constraints. Considering the structure and the performance of the steering mechanism. We set a range for the change of AoA. At the same time, for the hypersonic morphing aircraft, the leading edge sweep angle is designed according to the detonation shock generated by the head cone at a fixed Mach number. Therefore, for the Mach number of the two morphing times, the design Mach number is used as benchmark, and the Mach number can change within a certain range. In the ballistic constraint, in order to simplify the optimization problem, the ballistic end point constraint is mainly considered, that is, the height and speed of the descent phase. In the follow-up study, more constraints such as no-fly zones can be further considered.

D. MULTIOBJECTIVE OPTIMIZATION ALGORITHM

According to the multiobjective trajectory optimization model of the morphing aircraft established in the previous section, considering the possible conflict between the two objective functions, the range and the total heat absorption, in this paper the MOEA/D optimization algorithm is adopted to perform multiobjective optimization calculations on the model.

MOEA/D is based on the traditional aggregation method and decomposes MOP into multiple single-objective optimization problems [37]. The goal of each single-objective optimization problem is linear or non-linear weighted aggregation of all targets. The Euclidean distance based on the aggregation weight vector defines the neighbor relationship of the sub-problems. If the weight vectors of the two subproblems are relatively close, they are neighbors. The optimization of each sub-problem mainly uses the information of its neighbor sub-problems. Compared with the traditional decomposition method, MOEA/D uses the neighboring subproblems to collaborate with each other to simultaneously evolve all sub-problems. An approximation of PF is obtained through one time running to improving the solution efficiency. Compared with the classical evolutionary algorithm, MOEA/D specifies the fitness value based on the decomposition method, and uses a uniformly distributed weight vector to obtain a more uniformly distributed Pareto optimal solution.

If the Tchebycheff decomposition method is used, the original multiobjective optimization problem can be decomposed into N scalar optimization problems. Let $\lambda^1, \lambda^2, \ldots, \lambda^N$ be a set of weight vectors uniformly distributed, z^* is the reference point, then the objective function of the J-th sub-problem is as Equation (15).

$$g^{te}(x \left| \lambda^j, z^* \right.) = \max_{1 \le i \le m} \left\{ \lambda_i^j \left| f_i(x) - z_i^* \right| \right\} \tag{15}$$

where $\lambda^j = \left(\lambda_1^j, \ldots, \lambda_m^j\right)^T$. MOEA/D minimizes all these N objective functions simultaneously in a single run.

Since g^{te} is continuous with respect to λ, when λ^i and λ^j are close to each other, then the optimal solution of $g^{te}(x \left| \lambda^i, z^* \right.)$ should be close to the optimal solution of $g^{te}(x \left| \lambda^j, z^* \right.)$, so any information about g^{te} that is close to λ^i is helpful for optimizing $g^{te}(x \left| \lambda^i, z^* \right.)$. In MOEA/D, the adjacent sub-problems are defined according to the distances of the weight vectors λ^i, The neighborhood of the i th subproblem consists of all the subproblems with the weight vectors from the neighborhood of λ^i. The population is composed of the best solution found so far for each subproblem. Only the current solutions to its neighboring subproblems are exploited for optimizing a subproblem in MOEA/D.

The algorithm generally includes three steps such as initialization, updating, and stopping in each generation.

Step 1) Initialization:

Step 1.1) Set the number of evolution iterations $t^{\max}$, the number of subproblems N, the weight vector $\lambda^1, \ldots, \lambda^N$, and the number of neighbor vectors T.

Step 1.2) Compute the Euclidean distances between any two weight vectors and then work out the T closest weight vectors to each weight vector.

Step 1.3) Generate an initial population $x^1, \ldots, x^N$ randomly or by a problem-specific method. Set $FV^i = F\left(x^i\right)$.

Step 1.4) Initialize $z = (z_1, \ldots, z_m)^T$ by a problem-specific method.

Step 2) updating:

For $i = 1, \ldots, N$, do the following steps,

Step 2.1) Reproduction: Randomly select two indexes k, l from neighboring vectors, and then generate a new solution y from x^k and x^l by using genetic operators.

Step 2.2) Improvement: Apply a problem-specific repair/improvement heuristic on y to produce y'.

Step 2.3) Update of z: For each $j = 1, \ldots, m$, if $z_j < f_j(y')$, then set $z_j = f_j\left(y'\right)$.

Step 2.4) Update of Neighboring Solutions: For each vector with index j in neighbor vectors, if $g^{te}\left(y' \left| \lambda^j, z\right.\right) \leq g^{te}\left(x^j \left| \lambda^j, z\right.\right)$,then set $x^j = y'$ and $FV^j = F\left(y'\right)$.

Step 3) stopping:

If the termination condition is met, the iteration ends and the optimize result is output; if the termination condition is not satisfied, continue the iterative calculation and transfer to step 2.1.

More detail of MOEA/D can be find in reference 30.

According to reference 30, it can be found that the major computational costs in MOEA/D is involved in Step 2. Step 2.1 and Step 2.2 just randomly pick two solutions for genetic operators and perform mutation operations on y, it requires $O(N)$ basic operations since Step 2 has N passes. Similarly, Step 2.3 performs $O(mN)$ comparisons and assignments, and Step 2.4 needs $O(mNT)$ basic operations since its major costs are to compute the values of g^{te} for T solutions and computation of one such a value requires $O(m)$ basic operations, and also there is a N since Step 2 has N passes. So the time complexity in each generation is $O(mNT)$, if the fixed number of generations is I, the time complexity of MOEA/D is $O(mNTI)$. In reference 30, MOEA/D is proved to be less complex than other multiobjective optimization algorithms.

V. AERODYNAMIC PERFORMANCE

A. THE LIFT-TO-DRAG RATIO AND WING EFFICIENCY

In the previous section, profiles of morphing aircraft got through different morphing modes based on the reference profile were discussed. In order to analyze the advantages and disadvantages of different morphing modes, it is necessary to analyze the aerodynamic performance. The aerodynamic characteristics are calculated by using the turbulent viscosity coefficient method to time-average the unsteady N-S equations, and the turbulent viscous coefficients are solved using the SST k-ω turbulence model [38].

Using the calculation methods above, the aerodynamic characteristics of the three different morphing modes are analyzed under supersonic and hypersonic flow conditions. The performance of different morphing modes are compared. Lift-to-drag ratio of different morphing modes under Mach 3 and 8 is shown in Fig.7 and Fig.8, variation of the control surfaces rotations are not considered in this paper. Each curve in these figures represent a specific profile, such as reference profile, telescopic wing morphing profile, etc. And the points on each curve represent the lift-to-drag ratio of a specific profile in different angle of attack. In both conditions, lift-to-drag ratio increases with AoA and reaches maximum at 10°, then starts to decrease. Within a certain range, the lift increases linearly with AoA. When AoA increases to the critical AoA, the lift coefficient will reach an extreme value. After the critical AoA is exceeded, the lift is rapidly reduced due to the rapid increase in airflow separation. In terms of drag, at small AoA, the induced drag is not large, and as AoA increases, the induced drag increases rapidly. With the change of lift and drag with AoA, the lift-to-drag ratio is firstly increased and then decreased. For the configuration discussed in this paper, the lift-to-drag ratio is maximized near 10°.

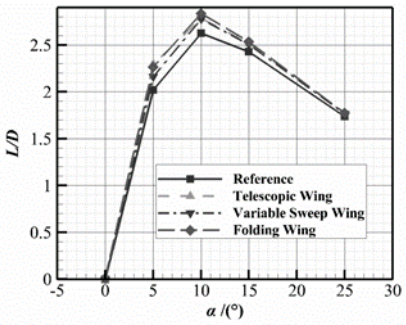

FIGURE 7. Lift-to-drag ratio under Mach 3.

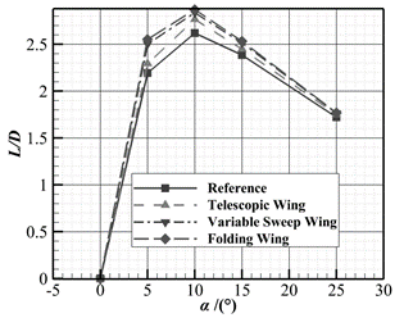

FIGURE 8. Lift-to-drag ratio under Mach 8.

Under Mach 3, when AoA is in the range of 5° to 15°, three morphing modes have significantly improved the lift-to-drag ratio compared to the reference profile. The lift-to-drag ratio of the three models reaches the maximum at around 10°, and the values are not much different. Under Mach 8, the lift-to-drag ratio of the telescopic morphing mode is lower than the

other two modes. When AoA is 5°, it is most evident from the figure. The obvious increase of the drag coefficient is the main reason for the low lift-to-drag ratio of the telescopic wing morphing mode. Unlike the variable sweep wing morphing mode and the folding wing morphing mode, the telescopic wing morphing mode mainly achieves the purpose of expanding the lift area by increasing the wingspan, it has also been widely used in the subsonic speed range. However, at high Mach number, the impact of the head cone's off-body shock wave on the telescopic wing is intensified, which reduces the lift-to-drag ratio.

Under AoA of 10° when the maximum lift-to-drag ratio is reached, the aerodynamic characteristics of the aircraft with different morphing modes in wide Mach domain is shown in Fig.9. All the three curves increase in supersonic condition and reach the peak around Mach 5, then start to decrease in hypersonic condition. When the aircraft is in hypersonic flow, the distance between the bow shock and the body decreases at higher Mach numbers, the mutual interference between the shock wave and the boundary layer is serious, the high-speed airflow is stagnated by the compression of the shock wave and has a strong friction with the surface of the aircraft.

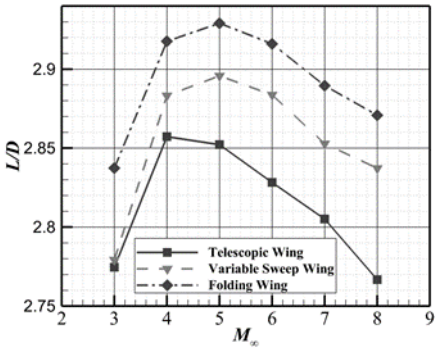

FIGURE 9. Lift-to-drag ratio under AoA 10° in wide Mach domain.

From the analysis of Fig.9, it can be seen that the overall lift-to-drag ratio performance of the telescopic wing morphing mode is worse than that of the other two modes. Compared with the other two morphing modes, the expansion ratio of the telescopic wing morphing mode is larger. Under the same conditions, it has greater wave resistance and friction resistance, therefore, with the increase of Mach number, the decreasing trend of lift-to-drag ratio at AoA of 10° becomes more obvious. Compared with the other two morphing modes at the hypersonic stage, it is in a clear disadvantage.

In order to investigate the contribution of wings to the lift-to-drag ratio of the aircraft under different morphing modes, the aerodynamic characteristics of the morphing wings of the three morphing modes are analyzed separately to study the wing efficiency of each morphing mode, to find which morphing mode can improve the aircraft lift-drag ratio and range more effectively. The morphing wing area of different morphing modes is measured, the lift-to-drag ratio is analyzed, and the lift-to-drag ratio of the unit wing area is defined as the wing efficiency η, as in Equation (16), S is the area of the wing.

$$\eta = \frac{L/D}{S} \tag{16}$$

Because the aircraft studied in this paper relies on morphing wing to increase lift, the larger the lift wing area, the higher the overall lift-to-drag ratio of the aircraft. Among them, the area of telescopic wing is not much different from the variable sweep wing, and the folding wing has a larger wing area. From Table 1, it can be seen that as the Mach number increases, the wing efficiency decreases, and in the three morphing modes, the wing efficiency is highest in the variable sweep wing morphing mode. In addition, the profile of telescopic wing morphing mode is affected by the shock wave from the nose cone after the wingspan is enlarged, the overall aerodynamic performance is poor, and the wing efficiency is the lowest. Compared with the variable sweep wing morphing mode, the folding wing morphing mode increases the overall lift-to-drag ratio with a larger lift area, so the wing efficiency is lower.

TABLE 1. Comparison of wing efficiency.

Mach \ Mode	Telescopic	Variable sweep	Folding
3	5.771	6.054	5.592
6	5.351	5.933	5.489
8	4.979	5.900	5.454

B. STABILITY ANALYSIS

The purpose of morphing is various, not only to improve the lift-to-drag ratio, but also to change the stability characteristics of the aircraft, and it has an exploration significance for the development of different ways of manipulation.

The morphing aircraft in this paper only deforms the lift wing, keeps the air rudders unchanged, and the wing morphing may affect the stability characteristics of the aircraft. Therefore, the longitudinal stability characteristics of the aircraft under the three morphing modes have been compared and analyzed in this paper.

The static stability of an aircraft is the ability of an aircraft to return to equilibrium without manipulation, after the aircraft has been deviated from equilibrium by external disturbances. The partial derivative m_Z^α represents the magnitude and direction of the pitching moment coefficient caused by the unit angle of attack, which characterizes the longitudinal static stability of the aircraft, which can be calculated through Equation (17) based on the simulation result. In Equation (17), c_Y represent the lift coefficient, x_g and x_F represent the position of center of gravity and center of pressure, L is the length of the aircraft. The three different morphing modes with different Mach numbers are shown in Table 2.

$$m_Z^\alpha = c_Y \left(x_g - x_F\right)/L \tag{17}$$

TABLE 2. Variations in m_Z^α with different Mach numbers.

Mach \ Mode	Telescopic	Variable sweep	Folding
3	-0.002859	-0.002857	-0.002833
6	-0.002174	-0.001976	-0.002032
8	-0.002058	-0.001941	-0.001960

As can be seen from the data in Table 2, the longitudinal static stability of the aircraft under the three morphing modes is all of high quality. Under the supersonic flow, the three morphing modes have almost the same value of m_Z^α. At hypersonic speed, the absolute value of m_Z^α of the telescopic wing morphing mode is 6% larger than the variable sweep wing morphing mode and the static stability is better. This is due to the backward extension of the telescopic wing and the backward movement of the pressure center.

For a statically stabilized aircraft with air rudders on the rear, when the rudders are deflected upwards by an angle of $\delta_Z < 0$, a downward manipulative force will be generated on the rudder surface and a rising moment $M_Z(\delta_Z) > 0$ relative to the center of gravity of the aircraft will be formed, so that AoA increases, the lift generated by the increase in AoA forms a bowing moment to the center of gravity. When the moment balance is reached, α and δ_Z satisfy the following relationship:

$$\left(\frac{\delta_z}{\alpha}\right)_b = -\frac{m_z^\alpha}{m_z^{\delta_z}} \tag{18}$$

In the equation above, $m_Z^{\delta Z}$ is the steering moment factor caused by the unit deflection of the rudder, which is called the rudder effectiveness. The rudder effectiveness of three morphing modes at different Mach numbers is shown in Table 3.

TABLE 3. Variations in $m_Z^{\delta Z}$ with different Mach numbers.

Mach \ Mode	Telescopic	Variable sweep	Folding
3	-0.001606	-0.001616	-0.001526
6	-0.000758	-0.000688	-0.000630
8	-0.000529	-0.000455	-0.000414

It can be seen from Table 3 that the rudder effectiveness of telescopic wing morphing mode under the hypersonic condition is higher than that of the other two morphing modes. When the Mach number is 8, the rudder effectiveness has the largest difference, the rudder effectiveness of the telescopic wing morphing mode is 14% and 22% higher than that of the variable sweep wing morphing mode and the folding wing morphing mode, respectively. This is due to the significant increase in the wingspan of the telescopic wing, so the impact of the telescopic wing tip shock on the air rudder is very small. For the variable sweep wing morphing mode and the folding wing morphing mode, the rudder effectiveness decreases rapidly as the Mach number increases, this is because the lift wings of the two modes are located in front of the air rudder, and the trailing edge is closer to the aircraft. As the Mach number increases, the rudder disturbance increases and the rudder efficiency is adversely affected. In the folding wing morphing mode, the overall wingspan of the lift wing becomes larger, and the shock wave generates at the trailing edge of the wing has greater influence on the air rudders, and the rudder effectiveness is lower than that of the variable sweep wing morphing mode.

C. ANALYSIS OF MORPHING MODES

According to the analysis, the aerodynamic performance of variable sweep wing morphing mode and folding wing morphing mode is better than telescopic wing morphing mode in hypersonic flow condition. Among the three morphing modes, variable sweep wing morphing mode has the highest wing efficiency. The static stability and rudder effectiveness of telescopic wing morphing mode under hypersonic flow condition are higher than those of the other two morphing modes. The rudder effectiveness of the folding wing morphing mode is significantly lower than that of the variable sweep wing morphing mode. In general, each morphing mode has its own pros and cons, for the sake of simplicity, the variable sweep wing morphing mode is selected for a detailed optimization and analysis.

Considering the launch constraint of the aircraft and the flight environment, in order to increase the range of the aircraft in the non-powered glide trajectory, a two-stage variable sweep wing morphing mode is adopted for the following research. After the reentry and pulling up into the glide phase of the trajectory, a variable sweep wing morphing occurs during the hypersonic phase, and a second morphing occurs when the flying speed drops to supersonic speed. The sweep angles of the morphing wing are determined according to the cone shock angles in selected conditions, in this paper are Mach 6 and Mach 3.

VI. OPTIMIZATION RESULTS AND ANALYSIS

A. DESIGN VARIABLES AND SIMULATION CONDITIONS

The Mach numbers of two morphing timing $\boldsymbol{M}_1$ and $\boldsymbol{M}_2$ are chosen as design variables, and the angle of attack of three phases of the trajectory changes linearly, which is determined by AoA of starting point and end point of each phase. The baseline value and range of each parameter is shown in Table 4. The parameters at the point of pulling up are shown in Table 5, and when the altitude comes to 20 km, or the Mach number reduced to 2, simulation is terminated.

B. OPTIMAL PARAMETER DESIGN AND RESULT ANALYSIS

MOEA/D is used to do the multiobjective glide trajectory optimization for the varied sweep wing morphing aircraft. The decomposition method adopts Tchebycheff method, the population size is 200, the number of iteration steps is 300, and the neighbor scale is 20.

TABLE 4. Design variables.

Parameters	M_1	M_2	α_1/°	α_2/°	α_3/°	α_4/°	α_5/°	α_6/°
Baseline value	6	3	5	15	5	15	5	15
Lower limit	5.5	2.5	5	5	5	5	5	5
Upper limit	6.5	3.5	15	15	15	15	15	15

TABLE 5. Beginning conditions of glide trajectory.

Parameters	Value	Parameters	Value
Horizontal height /km	32.5	Mass of aircraft / kg	1200
Geocentric latitude /°	0	Velocity /(m/s)	3240
Geocentric longitude /°	0	Velocity Angle /°	0

TABLE 6. Design variable and objective function values of optimal solution.

Parameters	M_1	M_2	α_1/°	α_2/°	α_3/°	α_4/°	α_5/°	α_6/°	R/km	Q/(MW/m^2)
Solution1	5.5	2.5	15	15	15	15	15	15	775.4	202.7
Solution2	5.55	2.68	8.71	9.00	8.25	9.84	15	8.14	899.5	335.8
Solution3	5.5	2.5	14.94	9.83	11.09	10.65	15	7.35	864.0	257.1

Based on the beginning conditions, the glide range with baseline values of the design variable is 733.11 km, and the total heat of the leading edge is 335.84 Mw/m^2.

The approximate PF of the optimization results is shown in Fig.10. MOEA/D used the Tchebycheff decomposition method, therefore, the two ends of the Pareto front corresponded to the best of two single-objective optimal solutions. As can be seen from Fig.10, there is a clear conflict between the two objective functions, the range and the total heat absorption. The specific parameters and objective function values of the two single-objective optimal solutions are shown in solution 1 and solution 2 of Table 6, and solution 3 is a selected multiobjective optimization solution, as noted in Fig10. Baseline value is also noted in the figure, as can be seen from the figure, baseline is not an optimal solution.

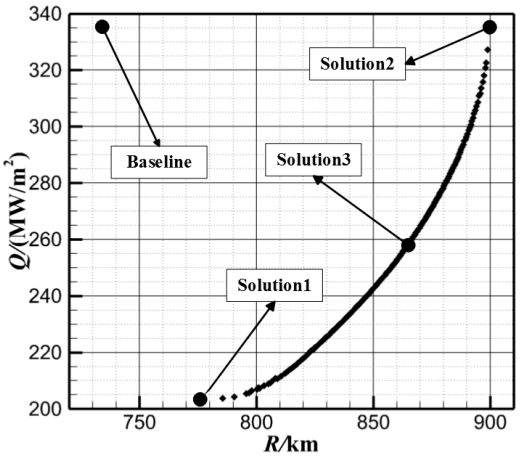

FIGURE 10. Pareto front of MOP for morphing aircraft.

The single-target optimal solution has the following features:

(1) Parameters of the total heat absorption minimum solution are listed in solution 1 of Table 6. In this solution, the total heat absorption of the leading edge of the morphing wing is the minimum, which is about 39.6% lower than baseline solution, and the range increases by 5.8%;

(2) The parameters of the maximum range solution are as shown in solution 2 of Table 6. In this solution, the range of the aircraft is the largest, about 22.7% higher than baseline solution, and the total heat absorption at the leading edge of the morphing wing is almost the same as baseline solution.

Compared single-target optimal solutions with baseline solution, both two single-target solutions have a significantly increase in range, and the total heat absorption is not greater than the baseline solution, which means that baseline solution is not on the Pareto front, it is not an optimal solution for the multiobjective problem.

Solution 3 is a selected multiobjective optimal solution, it can be found that solution 3 has an increase of 17.9% in range, a decrease of 23.4% in the total heat absorption compared to reference solution. Furthermore, the range decrease nearly 3.9% compared to the maximum range solution (solution 2), the total heat absorption increase nearly 26.8% compared to the minimum total heat absorption solution (solution 1). From the above analysis, the selected multiobjective optimization solution (solution 3) is a trade-off between the two objective functions. On the basis of the maximum range solution, 3.9% of the range is sacrificed, and the total heat absorption at the leading edge is reduced by approximately 23.4%.

The altitude-range curve sand the dynamic pressure-time curves of the three optimal solutions are shown in Fig.11 and Fig.12. Solution 1 has a wavy trajectory to maintain a high altitude, with a low density and pressure flight environment, the dynamic pressure is smallest in the three solutions as in Fig.12, leading to a low heat flux. Also, the wavy trajectory consumes more energy than the other two solutions, so the trajectory of solution 1 terminated at an altitude of 23.3 km with the shortest range. Solution 2 has a stable trajectory with

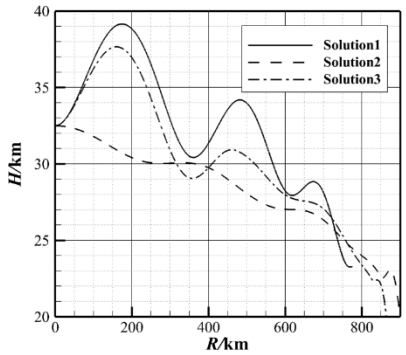

FIGURE 11. Altitude-range curves.

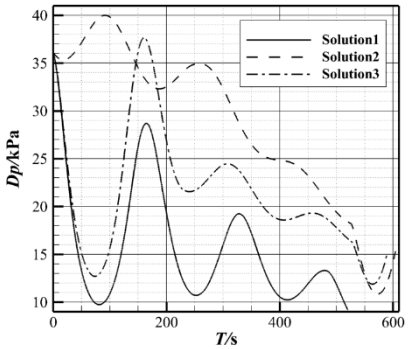

FIGURE 12. Dynamic pressure-time curves.

almost no extra action, so it has the longest range, however, the stable descend of the aircraft leads to high dynamic pressure as in Fig.12, and the heat flux is quite large. The trajectory of solution 3 is between solution 1 and 2, with an obvious rise of the trajectory, the heat flux condition has been ameliorated, and then the trajectory descends more stable, leading to a longer range, it can be seen clearly in Fig.13. For the sake of safety of the morphing mechanism, the vertical overload curves of all the three solutions are drawn in Fig.14, they are all within the allowable range to keep the morphing mechanism in good condition.

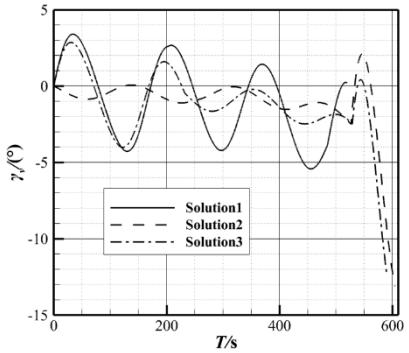

FIGURE 13. Velocity inclination angle-time curves.

Also, a brief comparison of the trajectory optimization result of all the three morphing modes is made in Table 7.

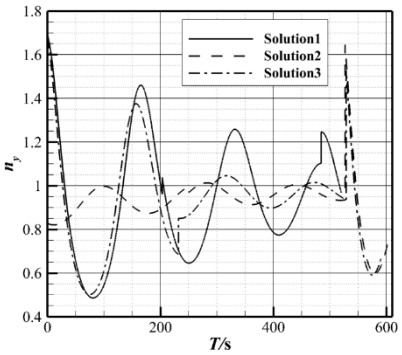

FIGURE 14. Overload-time curves.

TABLE 7. Comparison of trajectory optimization result of different morphing modes.

		Mode 1	Mode 2	Mode 3
Solution 1	$\boldsymbol{R}$/km	775.4	761.2	764.6
	$\boldsymbol{Q}$/(MW/m^2)	202.7	204.4	204.3
Solution 2	$\boldsymbol{R}$/km	899.5	878.6	900.3
	$\boldsymbol{Q}$/(MW/m^2)	335.8	336.0	343.1

As the variable sweep wing morphing mode, the sweep angles and the span of the wing of the other two morphing modes are determined according to the cone shock angles in Mach 6 and Mach 3.

In Table 7, variable sweep wing morphing mode is named as Mode 1, telescopic wing morphing mode is named as Mode 2, folding wing morphing mode is named as Mode 3. Both the total heat absorption minimum solution and the maximum range solution are listed in the table as Solution 1 and Solution 2. It can be seen from the table that the total heat absorption of all the three modes is almost the same, as the sweep angle of morphing wing is designed according the same condition, which will affect the heat flux significantly. The range of the trajectory of Mode 2 has an obvious difference compared to Mode 1 and Mode 3, it seems that the telescopic wing morphing mode has a poor performance in hypersonic and supersonic environment. Combine with the aerodynamic performance analysis in the previous sections, the variable sweep wing morphing mode seems to have a better overall performance.

In order to verify the effect of the variable sweep wing morphing mode, the same AoA instructions as the three optimization solutions are used to perform trajectory simulations of the reference aircraft without morphing and then compared the objective function values.

The objective function values of the above three optimization solutions and the objective function increment after adopting the variable sweep wing morphing mode are shown in Table 8, $\boldsymbol{R}$ and $\boldsymbol{Q}$ refer to range and total heat absorption of reference aircraft, ***Morph R*** and ***Morph Q*** refer to the increment after morphing compared to reference aircraft.

Through the comparison of the total heat absorption and the range with and without morphing, it can be concluded

TABLE 8. Objective function values of reference aircraft and increment after morphing.

	Solution1	Solution 2	Solution 3
R/km	764.50	823.51	777.77
Morph R	+1.43%	+9.23%	+11.09%
Q/(MW/m^2)	228.83	363.84	288.43
Morph Q	-11.42%	-7.71%	-10.86%

that the variable sweep wing morphing mode can increase the range of glide trajectory and decrease the total heat absorption of the leading edge of the wing; compared to single-target optimal solutions, in multiobjective solution, objective function values could be improved more significant and balanced. Also, the other two morphing modes can also get the same conclusion.

VII. CONCLUSION

Aiming at improving the range of the wing-body combination aircraft at hypersonic flow conditions and exploring the application of morphing technology in hypersonic aircraft, three morphing modes are mainly considered in this paper: telescopic wing, variable sweep wing and folding wing. The lift-to-drag ratio, wing efficiency, static stability and rudder effectiveness of different morphing modes have been analyzed and compared. Then a two-stage hypersonic morphing aircraft based on variable sweep wing is proposed for a detailed optimization and analysis.

Through the multiobjective trajectory optimization based on MOEA/D, it can be seen that the variable sweep wing morphing technology can increase the range, and decrease the total heat absorption of the leading edge of the wing of hypersonic aircraft significantly. In the selected multiobjective solution, the range improves 11.09%, and the total heat absorption reduces 10.86%, based on the range and the total heat absorption of the none-morphing hypersonic aircraft in the same conditions. Through a brief comparison of the trajectory optimization result of different morphing modes, it seems that the variable sweep wing morphing mode has a better overall performance. For further research, a detailed aerodynamic shape optimization of variable sweep wing morphing aircraft can be carried out. Also, the structural reliability of the morphing mechanism in hypersonic flow should be analyzed for the practical engineering application.

REFERENCES

[1] Y. Lu, Z. He, and Y. Lyu, "Morphing aircraft technology," *Aeronautical Manuf. Technol.*, vol. 33, no. 22, pp. 26–29, 2008.
[2] S. Barbarino, O. Bilgen, R. M. Ajaj, M. I. Friswell, and D. J. Inman, "A review of morphing aircraft," *J. Intell. Mater. Syst., Struct.*, vol. 22, no. 9, pp. 823–877, 2011.
[3] A. Rodriguez, "Morphing aircraft technology survey," in *Proc. AIAA Aerosp. Sci. Meeting Exhibit*, 2007, pp. 1–6, Art. no. AIAA2007-1258.
[4] Y. He and B. Wang, "The research status of morphing aircraft abroad," *Aerodyn. Missile J.*, vol. 43, no. 10, pp. 49–55, 2013.
[5] C. Duan and G. Zhang, "Research and development of tactical missile with morphing wing," *Aeronautical Sci., Technol.*, vol. 18, no. 1, pp. 18–21, 2011.
[6] M. I. Friswell, "Morphing aircraft: An improbable dream," in *Proc. Conf. Smart Mater. Adapt. Struct. Intell. Syst.*, 2014, pp. 1–7, Art. no. 7754(SMASIS2014-7754).
[7] R. M. Ajaj, C. S. Beaverstock, and M. I. Friswell, "Morphing aircraft: The need for a new design philosophy," *Aerosp. Sci., Technol.*, vol. 49, pp. 154–166, Feb. 2016.
[8] J. Sun, Q. Guan, Y. Liu, and J. Leng, "Morphing aircraft based on smart materials and structures: A state-of-the-art review," *J. Intell. Mater. Syst., Struct.*, vol. 27, no. 17, pp. 2289–2312, 2016.
[9] D. Bye and P. McClure, "Design of a morphing vehicle," in *Proc. AIAA/ASME/ASCE/AHS/ASC Struct. Dyn., Mater. Conf.*, 2007, p. 1728.
[10] J. Flanagan, R. Strutzenberg, R. Myers, and J. Rodrian, "Development and flight testing of a morphing aircraft, the NextGen MFX-1," in *Proc. AIAA/ASME/ASCE/AHS/ASC Struct., Dyn., Mater. Conf.*, 2013, p. 1707.
[11] T. A. Weisshaar, "Morphing aircraft systems: Historical perspectives and future challenges," *J. Aircraft*, vol. 50, no. 2, pp. 337–353, 2013.
[12] J.-S. Bae, T. M. Seigler, and D. J. Inman, "Aerodynamic and static aeroelastic characteristics of a variable-span morphing wing," *J. Aircraft*, vol. 42, no. 2, pp. 528–534, 2005.
[13] J. S. Bae, T. M. Seigler, D. Inman, and I. Lee, "Aerodynamic and aeroelastic considerations of a variable-span morphing wing," in *Proc. AIAA/ASME/ASCE/AHS/ASC Struct., Dyn. Mater. Conf.*, 2006, p. 1726.
[14] Q. Chen, P. Bai, and F. Li, "Morphing aircraft wing variable-sweep: Two practical methods and their aerodynamic characteristics," *Acta Aerodynamica Sinica*, vol. 30, no. 5, pp. 658–663, 2012.
[15] F. Gao, "Modeling and optimal flight scheme design of new concept morphing aircraft," M.S. thesis, School Astronaut., Harbin Inst. Technol., Harbin, China, 2014.
[16] L. Huanhuan, "Optimal flight trajectory design of new concept morphing aircraft," M.S. thesis, School Astronaut., Harbin Inst. Technol., Harbin, China, 2015.
[17] J. Guo *et al.*, "Dynamics modeling and characteristic analysis for vehicle with asymmetric span morphing wing," *J. Syst. Eng. Electron.*, vol. 38, no. 8, pp. 1951–1957, 2016.
[18] M. Leahy, "Multidisciplinary design optimization of a morphing wingtip concept with multiple morphing stages at cruise," M.S. thesis, Dept. Mech. Ind. Eng., Univ. Toronto, Toronto, ON, Canada, 2013.
[19] D. A. Burdette, G. K. Kenway, and J. Martins, "Aerostructural design optimization of a continuous morphing trailing edge aircraft for improved mission performance," in *Proc. AIAA/ISSMO Multidisciplinary Anal. Optim. Conf.*, 2015.
[20] F. Afonso, J. Vale, F. Lau, and A. Suleman, "Performance based multidisciplinary design optimization of morphing aircraft," *Aerosp. Sci., Technol.*, vol. 67, pp. 1–12, Aug. 2017.
[21] Z. He, M. Yin, and Y.-P. Lu, "Tensor product model-based control of morphing aircraft in transition process," *Proc. Inst. Mech. Eng. G, J. Aerosp. Eng.*, vol. 230, no. 2, pp. 378–391, 2016.
[22] F. Michaud, H. Dalir, and S. Joncas, "Structural design and optimization of an aircraft morphing wing: Composite skin," *J. Aircraft*, vol. 5, no. 1, pp. 195–211, 2018.
[23] O. S. Gabor, A. Koreanschi, R. M. Botez, M. Mamou, and Y. Mebarki, "Numerical simulation and wind tunnel tests investigation and validation of a morphing wing-tip demonstrator aerodynamic performance," *Aerosp. Sci., Technol.*, vol. 53, pp. 136–153, Jun. 2016.
[24] A. Koreanschi *et al.*, "Optimization and design of an aircraft's morphing wing-tip demonstrator for drag reduction at low speed, Part I—Aerodynamic optimization using genetic, bee colony and gradient descent algorithms," *Chin. J. Aeronaut.*, vol. 30, no. 1, pp. 149–163, 2017.
[25] A. Koreanschi *et al.*, "Optimization and design of an aircraft's morphing wing-tip demonstrator for drag reduction at low speeds, Part II—Experimental validation using infra-red transition measurement from wind tunnel tests," *Chin. J. Aeronaut.*, vol. 30, no. 1, pp. 164–174, 2017.
[26] A. Ermakova and I. Dayyani, "Shape optimisation of composite corrugated morphing skins," *Compos. B, Eng.*, vol. 115, pp. 87–101, Apr. 2017.
[27] I. Dayyani, A. D. Shaw, E. I. S. Flores, and M. I. Friswell, "The mechanics of composite corrugated structures: A review with applications in morphing aircraft," *Compos. Struct.*, vol. 133, pp. 358–380, Dec. 2015.
[28] S. La, W. Y. Joe, M. Akbar, and B. Alsaidi, "Surveys on skin design for morphing wing aircraft: Status and challenges," in *Proc. AIAA Aerosp. Sci. Meeting*, 2018, p. 0315.
[29] K. Deb, A. Pratap, S. Agarwal, and T. Meyarivan, "A fast and elitist multiobjective genetic algorithm: NSGA-II," *IEEE Trans. Evol. Comput.*, vol. 6, no. 2, pp. 182–197, Apr. 2002.

[30] Q. Zhang and H. Li, "MOEA/D: A multiobjective evolutionary algorithm based on decomposition," *IEEE Trans. Evol. Comput.*, vol. 11, no. 6, pp. 712–731, Dec. 2007.
[31] Z. Feng, Q. Zhang, Q. Tang, T. Yang, and J. Ge, "Control-structure integrated multiobjective design for flexible spacecraft using MOEA/D," *Struct., Multidisciplinary Optim.*, vol. 50, no. 2, pp. 347–362, 2014.
[32] Z. Feng, Q. Zhang, Q. Zhang, Q. Tang, T. Yang, and Y. Ma, "A multiobjective optimization based framework to balance the global exploration and local exploitation in expensive optimization," *J. Global Optim.*, vol. 61, no. 4, pp. 677–694, 2015.
[33] A. Trivedi, D. Srinivasan, K. Pal, and T. Reindl, "A MOEA/D with non-uniform weight vector distribution strategy for solving the unit commitment problem in uncertain environment," in *Artificial Life and Computational Intelligence*. Cham, Switzerland: Springer, 2017.
[34] W. Peng, Z. Feng, T. Yang, and B. Zhang, "Trajectory multiobjective optimization of hypersonic morphing aircraft based on variable sweep wing," in *Proc. 3rd Int. Conf. Control Robot. Eng. (ICCRE)*, Apr. 2018, pp. 65–69.
[35] A. Tewari, *Atmospheric and Space Flight Dynamics*. Boston, MA, USA: Birkhüser, 2007.
[36] G. Jiang and L. Liu, *Heat Transfer of Hypersonic Gas and Ablation Thermal Protection*. Beijing, China: National Defend Industry Press, 2003.
[37] K. Deb and D. Kalyanmoy, *Multi-Objective Optimization Using Evolutionary Algorithms*. Hoboken, NJ, USA: Wiley, 2001.
[38] W. Liu, *Foundation of Computational Aerodynamics Parallel Programming*. Beijing, China: National Defend Industry Press, 2013.

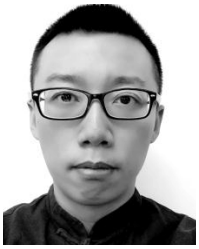

WUYU PENG was born in Mianyang, Sichuan, China, in 1990. He received the B.S. degree in weapons systems and engineering from the Nanjing University of Science and Technology, Nanjing, in 2012, and the M.S. degree in aeronautical and astronautical science and technology from the National University of Defense Technology, Changsha, in 2015. From 2008 to 2012, he was a student with the Nanjing University of Science and Technology. Since 2012, he has been a student with the National University of Defense Technology. His research interests in overall design and optimization of flight vehicles.

TAO YANG was born in Changde, Hunan, China, in 1962. He received the B.S. and M.S. degrees in solid rocket engine technology from the National University of Defense Technology, Changsha, in 1989, and the Ph.D. degree in ballistics from the Nanjing University of Science and Technology, Nanjing, in 1992. From 1992 to 1994, he was a Lecturer with the National University of Defense Technology, where he was any Associate Professor from 1994 to 2001, and a Professor, since 2001. His research interests include overall design and optimization of flight vehicles, aerospace propulsion theory, and engineering.

ZHIWEI FENG was born in Linfen, Shanxi, China, in 1984. He received the B.S. (aerospace engineering), M.S., and Ph.D. degrees in mechanics from the National University of Defense Technology, Changsha, in 2006, 2008, and 2014, respectively, where he is a Lecturer, since 2014. His research interests include aerodynamic design and multi-objective optimization of flight vehicles.

QINGBIN ZHANG was born in Datong, Shanxi, China, in 1975. He received the B.S., M.S. (mechanics), and Ph.D. degrees in aeronautical and astronautical science and technology from the National University of Defense Technology, Changsha, in 1996, 1999, and 2003, respectively where he was a lecturer, from 2003 to 2005, and an Associate Professor, since 2006. His research interests include multi-objective optimization, space nets, and parachute deployment.